ChemComm

Accepted Manuscript

This article can be cited before page numbers have been issued, to do this please use: Y. Liu, G. Liu, H. Xu, Y. Zheng, Y. Huang, S. Li and J. Li, *Chem. Commun.*, 2019, DOI: 10.1039/C9CC02006C.

ROYAL SOCIETY OF CHEMISTRY

rsc.li/chemcomm

View Article Online
DOI: 10.1039/C9CC02006C

COMMUNICATION

Low-Temperature Synthesized $Li_4Mn_5O_{12}$-Like Cathode with Hybrid Cation- and Anion-Redox Capacities

Yang Liu[a,b], Guang Liu[a,b], Hui Xu[a,b], Yuheng Zheng[a,b], Yunhui Huang[a,b], Sa Li[a,b*] and Ju Li[c*]

Received 00th January 20xx,
Accepted 00th January 20xx

DOI: 10.1039/x0xx00000x

Li-rich spinel $Li_4Mn_5O_{12}$, aka $Li(Mn_{5/3}Li_{1/3})O_4$ where 1/6 of the Mn of the classical $LiMn_2O_4$ spinel structure are replaced by Li, historically only shows reversible cation-redox reaction at a voltage of ~3 V versus Li+/Li, with theoretical capacity of 135.5 mAh g-1. However, we found that a simple 400°C solid-state synthesis method gives a $Li_4Mn_5O_{12}$-like nanoparticulate cathode that yields significant reversible hybrid cation- and anion-redox capacities. With ~ 40% oxygen anion-redox capacity at ~4 V versus Li+/Li, a high specific capacity of 212 mAh g-1 was achieved. Stable cycling was achieved at current density 100 mA g-1, and a capacity of 153 mAh g-1 still remained after 145 deep cycles. Full-cell cycling of this cathode against a lithium-tin alloy anode is demonstrated. The reversible anion-redox contribution is attributed to the tiny particle size (<10nm) which facilitates electron tunneling, and possible random solid-solution in $Li(Mn_{5/3}Li_{1/3})O_4$ lattice, due to the low synthesis temperature of 400°C.

Although spinel $Li_4Mn_5O_{12}$ is cost-effective[1] and environment-friendly without the expensive and toxic Co or Ni, it has significant challenges to meet the demand of rechargeable batteries. Among them, the relatively low specific capacity has been a bottleneck ever since it was initially reported by M.M. Thackeray two decades ago.[2, 3] Starting with $Li_4^+Mn_5^{4+}O_{12}^{2-}$, because the Mn ions are already tetravalent, delithiation cannot occur[4] without concomitant change of the average oxygen valence as $Li_{4-m}^+Mn_5^{4+}O_{12}^{(2-a)-}$, where $a=m/12 \geq 0$ track the degree of oxygen anion-redox at around 4 V *vs.* Li^+/Li.[5-7] This was reportedly very difficult, or at least the capacity is highly irreversible. Upon first net lithiation, reversible capacity did emerge as $Li_4^+Mn_5^{4+}O_{12}^{2-} \leftrightarrow Li_{4+p}^+Mn_5^{(4-c)+}O_{12}^{2-}$, where $c=p/5 \geq 0$ track the degree of transition-metal cation-redox. This part of the capacity at around 3 V *vs.* Li^+/Li is practically seen to be reversible, and the spinel structure could be maintained as long as $p \leq 2.5$ ($c \leq 0.5$, $Li_{6.5}^+Mn_5^{3.5+}O_{12}^{2-}$), which gives a theoretical capacity of 135.5 mAh g^{-1}. If p is extended to 3 (c=0.6, $Li_7^+Mn_5^{3.4+}O_{12}^{2-}$), then the cation-redox theoretical capacity would rise to 162.6 mAh g^{-1}, but cyclability could be poor due to Jahn-Teller distortion induced phase transformation. In addition to low capacity and low voltage (135.5 mAh g^{-1} at 3 V), from the stand-point of making practical Li-matched full cell using $Li_4Mn_5O_{12}$ cathode against graphite anode, the following troubles must be considered: (a) one must use pre-lithiated graphite or other lithium source to supply additional cyclable lithium for the first net lithiation $Li_4^+Mn_5^{4+}O_{12}^{2-} \rightarrow Li_{4+p}^+Mn_5^{(4-c)+}O_{12}^{2-}$, (b) there is going to be some Mn-ion dissolution into the liquid electrolyte, which attacks the graphite anode viciously. For these reasons, $Li_4Mn_5O_{12}$ has not been considered as an attractive cathode material. Here, however, we will show that by a low-temperature synthesis at 400°C, we can make a nanostructured $Li_4Mn_5O_{12}$-like material with both *p*,*c*-contribution (Mn cation redox) and *m*,*a*-contribution (O anion redox), giving a total *reversible* capacity of 212 mAh g^{-1}. Furthermore, by pairing with a pre-lithiated Sn metal anode in a standard carbonate electrolyte, the dissolved Mn-ion attack on anode seems to be less of a problem. This enables stable cycling of a Li-matched full cell based on $Li_4Mn_5O_{12}$-like cathode for more than 100 cycles.

In previous reports, Takada *et al* had synthesized a well-crystallized $Li_4Mn_5O_{12}$ with a rechargeable capacity of about 135 mAh g^{-1} at a voltage of 2.5 ~ 3.6 V for only 10 cycles.[8] Jiang *et al* had reported that $Li_4Mn_5O_{12}$ prepared by spray-drying could deliver a discharge capacity of 157.8 mAh g^{-1} at a voltage range of 2.4 ~ 3.7 V and maintained 76% capacity retention after 80 cycles.[9] Fu *et al* found that $Li_4Mn_5O_{12}$ with hierarchical porous nano/micro structure had a capacity of 161 mAh g^{-1} at a voltage range of 2.0 ~ 3.5 V and it maintained about 89 mAh g^{-1} after 100 cycles at 0.5 C.[10] In most studies, the main capacity appears to originate from *p*,*c*-contribution (Mn cation redox) of $Li_4Mn_5O_{12} + 2.5\,e^- + 2.5\,Li^+ \rightarrow Li_{6.5}Mn_5O_{12}$ at a voltage of ~ 3 V *vs.* Li^+/Li, and the four initial lithium ions were not active during charge/discharge process. Moreover, doping strategies were also tried to enhance energy density of $Li_4Mn_5O_{12}$, and the operating voltage was increased to 4.7 V although there was no significant improvement in capacity.[11]

Inspired by recent understanding of reversible oxygen anion-redox in cathode materials, it behooves one to activate the anion-redox contributions and pursue hybrid cation- and anion-redox (HAC) capacities in cathode materials to boost the energy density.[5-7] While reversible $O^{2-} \leftrightarrow O^-$ (oxo $\leftrightarrow$ peroxo) transition has been demonstrated in Li-rich $Li_{1+x}M_{1-x}O_2$ with layered structure, such as $yLi_2MnO_3 \cdot (1-y)LiMO_2$ (M = Mn, Ni, Co mixture), there have been very few tries in spinel $Li_4Mn_5O_{12}$, also written as $Li(Mn_{5/3}Li_{1/3})O_4$, where 1/6 of the Mn ions in the classical $LiMn_2O_4$ spinel structure are replaced by Li ions.[4,12] Generally speaking, there is a mixture of ionic and covalent bonding between cations (Li, Mn) and oxygen. While Li-O bonding is strongly ionic, Mn_{3d}/O_{2p} have significant orbital overlap and thus Mn-O has stronger covalent bonding flavor, which stabilizes O^{2-} and pushes $U^{eq}(O^{1-/2-})$ to higher voltages. However, with 1/6 of the Mn ions replaced by Li ions, the degree of ionic bonding increases, and as a result, $U^{eq}(O^{1-/2-})$ can move to lower voltages, at around 4 V *vs.* Li^+/Li. Thus oxygen ions can, in principle, deliver extra *m*,*a*-capacities, before the voltage gets so high (like > 5 V) that the Al current collector corrodes or the electrolyte decomposes too violently.[13]

[a] School of Materials Science and Engineering, Tongji University, Shanghai 201804, China
[b] Institute of New Energy for Vehicles, Tongji University, Shanghai 201804, China
[c] Department of Nuclear Science and Engineering and Department of Materials Science and Engineering, Massachusetts Institute of Technology, Cambridge, MA 02139, USA

View Article Online
DOI: 10.1039/C9CC02606C

Herein, we report a simple and scalable solid-state method to synthesize nanoscale $Li_4Mn_5O_{12}$-like particulates at low temperature. After an activation process, not only the cation-redox capacity at ~ 3 V *vs*. Li^+/Li originated from $Mn^{3.5+} \rightarrow Mn^{4+}$, but also the anion-redox capacity at ~ 4V *vs*. Li^+/Li provided by $O^{2-} \rightarrow O^-$ is obtained. The reaction proceeds theoretically as $Li_2Mn_5O_{12} + 4.5\,e^-(U) + 4.5\,Li^+(\text{electrolyte}) \leftrightarrow Li_{6.5}Mn_5O_{12}$. (1)

with a theoretical capacity of 243.9 mAh g^{-1}, where anion-redox contributes 44% (*m*=2, *a*=1/6, 108.4 mAh g^{-1}) and cation-redox contributes 56% (*p*=2.5, *c*=0.5, 135.5 mAh g^{-1}), and the reaction coordinate of equation (1) is kinked as illustrated in Fig. 1. In practice, a high discharge specific capacity of 212 mAh g^{-1} and energy density of 668 Wh kg^{-1} were achieved in half cells.

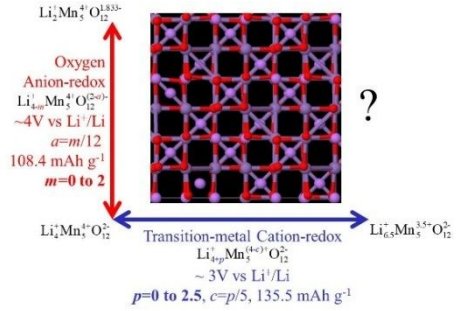

Fig. 1 Hybrid oxygen anion-redox and transition-metal cation-redox reaction coordinate of reaction (1): $Li_2^+Mn_5^{4+}O_{12}^{1.833-} \leftrightarrow Li_4^+Mn_5^{4+}O_{12}^{2-} \leftrightarrow Li_{6.5}^+Mn_5^{3.5+}O_{12}^{2-}$. The inset shows spinel $Li(Mn_{5/3}Li_{1/3})O_4$ with long-range order of the 1/6 Li_{Mn} substitutions. However, we believe our material may have significant disordering, or random solid solution, of these 1/6 Li_{Mn} substitutions, due to the low-temperature synthesis.

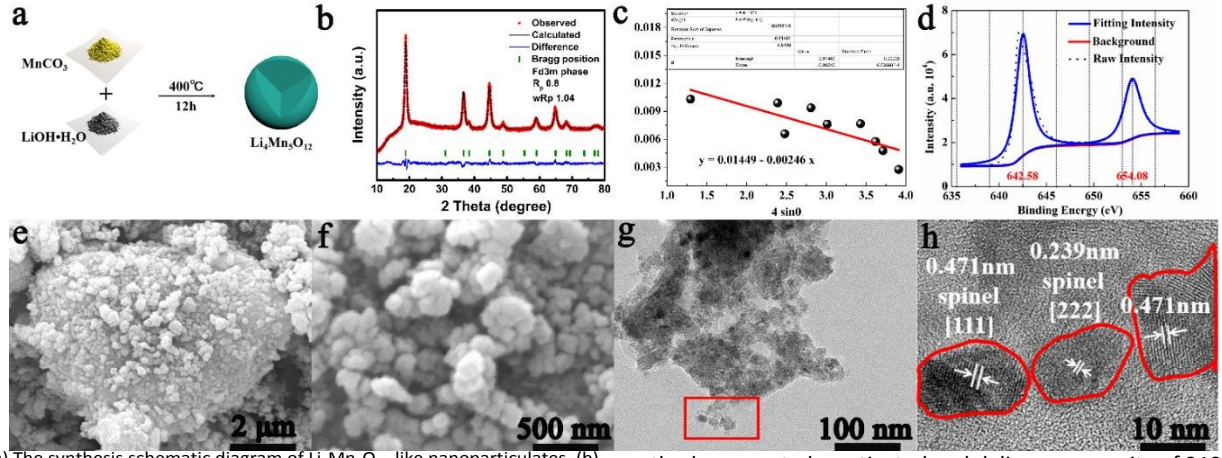

Fig. 2 (a) The synthesis schematic diagram of $Li_4Mn_5O_{12}$-like nanoparticulates, (b) Rietveld refinement XRD patterns, (c) Mn 2p XPS spectra, (d) and (e) SEM images, (f) and (g) TEM and HRTEM images of $Li_4Mn_5O_{12}$-like nanoparticulates, which self-assemble into secondary particles.

The low-temperature solid-state synthesis process is illustrated in Fig. 2a. $Li_4Mn_5O_{12}$-like cathode is prepared through a solid-state process, which is very simple and scalable. The as-obtained sample was then characterized by X-ray diffraction (XRD), and the XRD pattern (Fig. 2b) could be approximately indexed to $Li_4Mn_5O_{12}$ phase (JCPDS No. 46-0810). Based on Rietveld refinement, the lattice parameters of a monoclinic unit cell are *a*=8.128 Å and unit cell volume=537.130 $Å^3$, closely approaching the values reported by Takada, which confirms its $Li_4Mn_5O_{12}$-like motif.[14] From the Scherrer equation and Williamson-Hall analysis,[15] we found the particle size is 9.57 nm and the microstrain fluctuation (slope of broadening vs. 4sinθ) is ~ -0.00246 (as shown in Fig. 2c). The small but negative value of -0.00246 is unusual and means the particle sizes are so small that anisotropic surface stress and other factors give non-uniform strain distribution. The sub-10nm nanoparticulate nature (due to the low-*T* synthesis which prevented coarsening) is believed to play a key role in the ability to utilize the anion-redox capacity, since when Mn stays 4+ (the red leg of the reaction coordinate in Fig. 1), the electronic conductivity has to be low due to the lack of transition-metal polaron conduction (unlike the blue leg where there is an abundant mixture of Mn^{4+} and Mn^{3+}), and therefore one relies more on surface conduction and electron tunneling mechanisms, which favors smaller particles. On the other hand, while smaller particles have favorable kinetics, they also have more side reactions with the electrolyte, so an optimal particle size should exist.

X-ray photoelectron spectroscopy (XPS) was carried out (Fig. 2d) to identify the valence state of Mn. The fitting peaks are at 6 42.58 eV and 654.08 eV, that are the characteristic peaks of Mn^{4+} $2p_{3/2}$ and Mn^{4+} $2p_{1/2}$ respectively.[16, 17] The microstructure and morpholo gy of $Li_4Mn_5O_{12}$-like powders is also observed through field em ission scanning electron microscopy (FE-SEM) as shown in Fig. 2e an d 2f. Secondary microparticles with a diameter of around 5 μm could be seen (Fig. 2e) and closer observation in Fig. 2f reveals the secondary particles are self-assembled by primary nanoparticles. Such a hierarchical microstructure could also be identified by transmission electron microscopy (TEM), where subunits of ~ 20-100 nm agglomerated and formed ~ 5 μm particles. From the high-resolution transmission electron microscopy (HRTEM) image in Fig. 2h, interplanar spacing of 0.471 nm and 0.239 nm, which are corresponding to the [111] and [222] planes of spinel $Li_4Mn_5O_{12}$ structure, respectively, are identified. It is generally believed that such nano-sized crystallinity could effectively accommodate the strain of Jahn-Teller though slippage at the domain wall boundaries, and thus is beneficial to the stability of cathode material.[18-20]

The $Li_4Mn_5O_{12}$-like cathode was then electrochemically examined in coin cells. After an initial charging process $Li_4^+Mn_5^{4+}O_{12}^{2-} \rightarrow Li_{4-m}^+Mn_5^{4+}O_{12}^{(2-a)-}$ (that was largely abandoned in conventional samples due to lack of reversibility), $Li_4Mn_5O_{12}$-like cathode seems to be activated and delivers a capacity of 210 mAh g^{-1} (at 0.1 C) in the first discharge, when net-additional lithium was provide by the counter-electrode. In the following 20 cycles, the specific capacity increases gradually and reaches a maximum value of 212 mAh g^{-1} (a discharge energy density of 668 Wh kg^{-1}) at the 20th cycle. This would be impossible without the anion-redox *m*,*a*-contributions. As discussed before, since the tetravalent manganese ions cannot be oxidized, the first charge capacity of 82.6 mAh g^{-1} that we measured must arise from O-redox, which turns out to be highly reversible in the following cycles. The progress coordinate of reaction (1) contains a directional change as illustrated in Fig. 1 at $Li_4^+Mn_5^{4+}O_{12}^{2-}$, with one part given by the red anion-redox, and the other part given by the blue cation-redox leg. From the voltage profile, there is a plateau at 2.8 V *vs*. Li^+/Li that corresponds to lithium insertion into the octahedral sites of spinel $Li_4Mn_5O_{12}$ accompanied by the reduction of manganese ions $Li_4^+Mn_5^{4+}O_{12}^{2-} \leftrightarrow Li_{4+p}^+Mn_5^{(4-c)+}O_{12}^{2-}$. It is commonly believed that Jahn-Teller distortion has no chance of causing phase change/structural collapse as long as the oxidation state of manganese ions stays above 3.5.[4]

The CV curve (in Fig. 3c) also indicates that there are two lithium storage processes, corresponding to two redox peaks at ~ 2.8 V and

~ 4 V respectively during discharge process of $Li_4Mn_5O_{12}$-like cathode. Our $Li_4Mn_5O_{12}$-like cathode, which comes from a simple one-pot synthesis and was not optimized, can still maintain a capacity of 153 mAh g^{-1} and an energy density of 470 Wh kg^{-1} at room temperature after 145 cycles, as shown in Fig.3e. Interestingly, the capacity exhibits an increases trend at the initial 20 cycles, which we believe is associated with an activation process. From 30th cycle, the capacity starts to decay, possibly originated from the dissolution of manganese with a disproportionation reaction of $Mn^{3+}(solid) \rightarrow Mn^{4+}(solid) + Mn^{2+}(solution)$ and the onset of Jahn-Teller distortion at the end of discharge[4]. And the discharge potential of $Li_4Mn_5O_{12}$-like cathode is stable (at 3.1 V) during cycling, almost without any drop (in Fig. 3b). Thanks to the cubic structure of spinel $Li_4Mn_5O_{12}$ with three-dimensional Li diffusion channels, this cathode shows good rate performance with small impedance during cycling, as revealed in Fig. 3d.

Full cells were assembled by pairing the $Li_4Mn_5O_{12}$-like cathode against Li_xSn anode[37] and tested at a current density of 100 mA g^{-1} between 1.0 and 4.1 V *vs.* Li^+/Li at room temperature. As shown in Fig. 3f and 3g, the initial discharge capacity reaches 213 mAh g^{-1}. After 45 cycles, the capacity stabilizes at 204 mAh g^{-1} nearly without capacity attenuation.

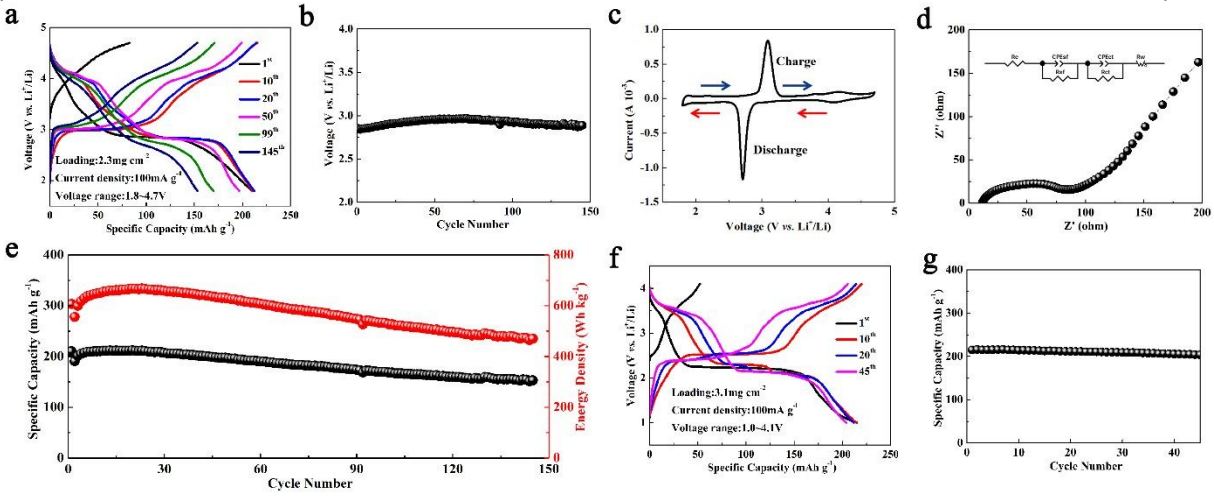

Fig. 3 (a) Charge/discharge curves of $Li_4Mn_5O_{12}$-like half cells from the 1st cycle to the 145th cycle at a current density of 100 mA g^{-1} among 1.8 ~ 4.7 V versus Li^+/Li at room temperature, (b) evolution of average discharge voltage during cycling, (c) CV curve of $Li_4Mn_5O_{12}$-like, (d) equivalent circuit model and Nyquist plots of $Li_4Mn_5O_{12}$-like, (e) cyclic performance of $Li_4Mn_5O_{12}$-like half cells, (f) charge/discharge curves of $Li_4Mn_5O_{12}$-like full cells from the 1st cycle to the 35th cycle at a current density of 100 mA g^{-1} among 1.0 ~ 4.1 V versus Li^+/Li at room temperature, (g) cyclic performance of $Li_4Mn_5O_{12}$-like full cells.

Based on the analysis above, the discharge capacities of $Li_4Mn_5O_{12}$-like cathode include hybrid cation- and anion-redox capacities. Here, we separate capacities into two parts in discharge curve of the 20th cycle, which are attributed to cation-redox and anion-redox respectively, as shown in Fig. 4a and 4b. The cation-redox process (Mn^{3+}/Mn^{4+}) covers area at about 3V *vs.* Li^+/Li. The capacities due to this process are 108.4 mAh g^{-1}, corresponding to a reaction of $Li_4Mn_5^{4+}O_{12}^{2-} + 2\,Li^+ + 2\,e^- \leftrightarrow Li_6Mn_5^{3.6+}O_{12}^{2-}$. The capacities attributed by anion-redox process are 103.6 mAh g^{-1}, which can be described as a reaction of $Li_4Mn_5^{4+}O_{12}^{2-} - 1.8\,Li^+ - 1.8\,e^- \leftrightarrow Li_{2.1}Mn_5^{4+}O_{12}^{1.84-}$. In Fig. S1, cation- and anion-redox capacities evolving over cycles are examined individually, where an anion-redox capacity increment during the first 30 cycles was observed, probably due to an activation process of oxygen. In the subsequent cycles, a slow decline that might be related to oxygen release could be found. Meanwhile, cation-redox capacity deteriorates gradually with prolonged cycling, which is possibly attributed to the dissolution of manganese and the damage of structure. In Fig. 4c, the derivative capacity vs. voltage of $Li_4Mn_5O_{12}$-like cathode is calculated by the data of the 20th cycle (presented in Fig. 4b). The main redox peaks are at ~ 2.8 V and ~ 4 V, which correspond to two reactions above mentioned. To clarify the underlying mechanism of anion-redox contribution, we conducted a DEMS test under a galvanostatic condition, as shown in Fig. 4d. During the first charging process, O_2 generates once potential exceeds 3.4 V, implying that there is O^{2-} oxidation. From the second cycle, no O_2 generation is detected, indicative of a possible existence of solid-state oxidized O^{2-}, which was further confirmed through XPS characterization (Fig. 4e). From the O1s spectrum, there is an obvious difference in oxidation state of oxygen atoms in $Li_4Mn_5O_{12}$-like cathode at different SOCs. Specifically, for pristine sample, a peak at 529.5 eV that corresponds to O^{2-} anions of the crystalline network[21, 22] and a peak at 532.1 eV that might be associated with weakly absorbed surface species such as CO_2, were observed. At 4.7 V, two new peaks occur. The peak at 531.1 eV is related to the onset of new component with lower electronic density of oxide ions than O^{2-} ions, indicating that O^{2-} ions are oxidized to O^-/O^{2-} or under-coordinated oxygen atoms[21]. And it disappears when sample is discharged to 1.8 V. We anticipate the reversible appearance/disappearance of 531.1 eV peak during the charge/discharge process reveals the reversibility of anion-redox reaction. Besides, the other peak at 533.2 eV corresponds to electrolyte oxidation[22, 23].

$Li_4Mn_5O_{12}$-like cathode could have excellent cost-performance ratio. Compared with the benchmark cathode materials, such as $LiFePO_4$, $LiCoO_2$, $LiNiO_2$ and $Li(Ni_xCo_yMn_{1-x-y})O_2$, our $Li_4Mn_5O_{12}$-like cathode can deliver a high capacity of 213 mAh g^{-1}, which behaves better than $LiFePO_4$ (162 mAh g^{-1}), $LiCoO_2$ (140 mAh g^{-1}), and $LiNi_{1/3}Co_{1/3}Mn_{1/3}O_2$ (200 mAh g^{-1}).[24-26] The cost of our cathode material is less than \$ 5.72 kg^{-1}, which is one fifth of the cost of $LiCoO_2$ (\$ 26.24 kg^{-1}), a quarter of the cost of $LiNi_{1/3}Co_{1/3}Mn_{1/3}O_2$ (\$ 20.99 kg^{-1}) and about one third of the cost of $LiFePO_4$ (\$ 12.72 kg^{-1}), as exhibited in Fig. 4f.

We are intrigued as to why our samples manifest reversible capacity $Li_4^+Mn_5^{4+}O_{12}^{2-} \rightarrow Li_2^+Mn_5^{4+}O_{12}^{1.833-}$ for hundreds of charge/discharge cycles. Besides the sub-10nm primary particle size (9.57 nm), we speculate that partial destruction of *chemical ordering* could also play a role. Recall that $Li_4Mn_5O_{12}$ is better understood as $Li(Mn_{5/3}Li_{1/3})O_4$, where 1/6 of the Mn sites in the classical $LiMn_2O_4$ spinel structure are replaced by Li ions.[4,12] However the $Li_4Mn_5O_{12}$ illustrated in Fig.1 is a *perfect compound* with chemical ordering, meaning those 1/6 Li_{Mn} substitutions are *perfectly long-range ordered*, and not an alloy. However, due to the 400°C low-*T* synthesis (most solid-state synthesis takes place at >700°C[27]), the ordering of these Li_{Mn} substitutions in our samples may not be perfect, and may form a random solid solution, despite the large agreement in XRD peaks in Fig. 2b with the reference crystal. That is, while the expression "Li-rich spinel $Li(Mn_{5/3}Li_{1/3})O_4$" should be correct as a chemical formula, those Li_{Mn} substitutions may have more randomized positions. We may also have Mn occupying some of the original tetrahedral Li sites of the classical $LiMn_2O_4$ spinel, or other kinds of local ionic disorders. For reference $Mn^{4+}{}_{tetrahedral/octahedral}$ has

Shannon-Prewitt crystal radius 0.53Å/0.67Å, while $Li^{+}_{tetrahedral/octahedral}$ has Shannon-Prewitt crystal radius 0.73Å/0.90Å.[28] This kind of random solid-solution behavior may explain the sloping voltage curve in the first charge in Fig. 3f.[29, 30, 31] Since the detailed Li-O-Mn and Li-O-Li geometries greatly affect the equilibrium oxygen redox potential[32, 33] as well as the internal charge-transfer rates (e.g. $O^{1-} \rightarrow O^{2-}$ & $Mn^{3+} \rightarrow Mn^{4+}$ together), we speculate this kind of occupation disorder and random-solution behavior with redox-activated dynamic rearrangements of ions[6] could facilitate oxygen redox, assisted of course also by the small particle size and electron tunneling.

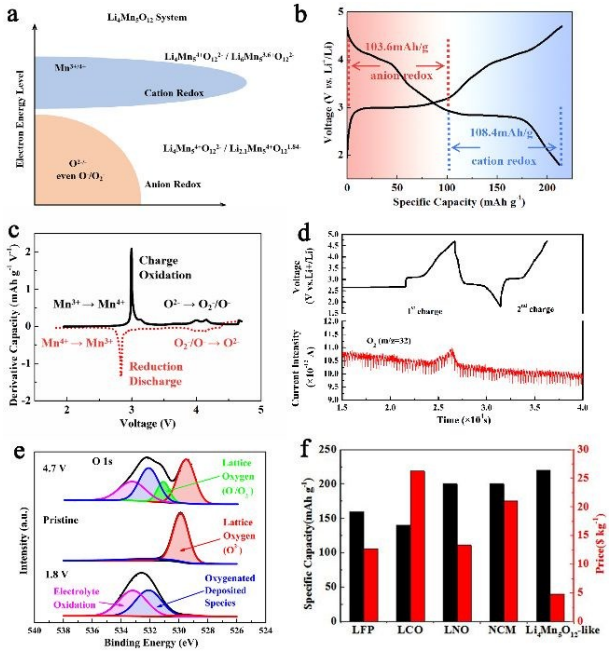

Fig. 4 (a) Schematic illustration of cation- and anion- redox processes in $Li_4Mn_5O_{12}$ system, (b) the distinguished cation- and anion-redox capacities in discharge curve of the 20th cycle respectively, (c) derivative capacity vs. voltage curve of $Li_4Mn_5O_{12}$ system during the 20th cycle, (d) DEMS analysis of $Li_4Mn_5O_{12}$-like cathode in half cell tested with a constant current density of 100 mA g^{-1} and a voltage window of 1.8 ~ 4.7 V versus Li^+/Li, (e) XPS spectra of pristine $Li_4Mn_5O_{12}$-like sample, sample charged 4.7 V and sample discharged to 1.8 V, (f) Capacities and price of $LiFePO_4$ (LFP), $LiCoO_2$ (LCO), $LiNiO_2$ (LNO), $Li(Ni_xCo_yMn_{1-x-y})O_2$ (NCM) and $Li_4Mn_5O_{12}$-like.

In summary, a cobalt-free $Li_4Mn_5O_{12}$-like nanoparticulate cathode, synthesized at a low temperature of 400°C (most solid-state synthesis of cathode materials occurs at above 600°C [10, 34-36]), demonstrates a high reversible capacity of 212 mAh g^{-1} with hybrid cation- and anion-redox contributions. Compared to commercial $LiFePO_4$, $LiCoO_2$, and $Li(Ni_xCo_yMn_{1-x-y})O_2$, it not only has lower cost, but also higher capacities. What is more, the cycling stability is also acceptable. The $Li_4Mn_5O_{12}$-like cathode maintains a capacity of 153 mAh g^{-1} after 145 cycles at a current density of 100 mA g^{-1}. The electrochemical performance of the full cell with this $Li_4Mn_5O_{12}$-like cathode and lithium tin alloy anode is impressive with a high capacity of 214 mAh g^{-1} and almost without any capacity fading after 45 cycles. Results above show that this Li-rich spinel, aka $Li(Mn_{5/3}Li_{1/3})O_4$, is attractive for further investigations as lithium-ion battery cathode.

References

1. A. R. Armstrong and P. G. Bruce, *Nature*, 1996, **381**, 499.
2. M. M. Thackeray, A. de Kock, M. H. Rossouw, D. Liles, R. Bittihn and D. Hoge, *Journal of The Electrochemical Society*, 1992, **139**, 363-366.
3. E. Ferg, R. Gummow, A. De Kock and M. Thackeray, *Journal of the Electrochemical Society*, 1994, **141**, L147-L150.
4. M. M. Thackeray, *Progress in Solid State Chemistry*, 1997, **25**, 1-71.
5. Z. Zhu, A. Kushima, Z. Yin, L. Qi, K. Amine, J. Lu and J. Li, *Nature Energy*, 2016, **1**, 16111.
6. W. E. Gent, K. Lim, Y. Liang, Q. Li, T. Barnes, S.-J. Ahn, K. H. Stone, M. McIntire, J. Hong and J. H. Song, *Nature communications*, 2017, **8**, 2091.
7. X. Rong, E. Hu, Y. Lu, F. Meng, C. Zhao, X. Wang, Q. Zhang, X. Yu, L. Gu and Y.-S. Hu, *Joule*, 2018.
8. T. Takada, H. Hayakawa, E. Akiba, F. Izumi and B. C. Chakoumakos, *Journal of power sources*, 1997, **68**, 613-617.
9. Y. Jiang, J. Xie, G. Cao and X. Zhao, *Electrochimica Acta*, 2010, **56**, 412-417.
10. Y. Fu, H. Jiang, Y. Hu, L. Zhang and C. Li, *Journal of Power Sources*, 2014, **261**, 306-310.
11. Z. Xie, H. Eikhuemelo, J. Zhao, C. Cain, W. Xu and Y. Wang, *Journal of The Electrochemical Society*, 2015, **162**, A1523-A1529.
12. M.-J. Lee, E. Lho, P. Bai, S. Chae, J. Li and J. Cho, *Nano letters*, 2017, **17**, 3744-3751.
13. L. Suo, W. Xue, M. Gobet, S. G. Greenbaum, C. Wang, Y. Chen, W. Yang, Y. Li and J. Li, *Proceedings of the National Academy of Sciences*, 2018, 201712895.
14. T. Takada, H. Hayakawa and E. Akiba, *Journal of Solid State Chemistry*, 1995, **115**, 420-426.
15. A. K. Zak, W. A. Majid, M. E. Abrishami and R. Yousefi, *Solid State Sciences*, 2011, **13**, 251-256.
16. V. Di Castro, G. Polzonetti, G. Contini, C. Cozza and B. Paponetti, *Surface and Interface Analysis*, 1990, **16**, 571-574.
17. B. J. Tan, K. J. Klabunde and P. M. A. Sherwood, *Journal of the American Chemical Society*, 1991, **113**, 855-861.
18. H. Wang, Y. I. Jang and Y. M. Chiang, *Electrochemical and Solid-State Letters*, 1999, **2**, 490-493.
19. Y. I. Jang, B. Huang, Y. M. Chiang and D. R. Sadoway, *Electrochemical and Solid-State Letters*, 1998, **1**, 13-16.
20. Y. Shao-Horn, S. A. Hackney, A. R. Armstrong, P. G. Bruce, R. Gitzendanner, C. S. Johnson and M. M. Thackeray, *Journal of The Electrochemical Society*, 1999, **146**, 2404-2412.
21. J.-C. Dupin, D. Gonbeau, P. Vinatier and A. J. P. C. C. P. Levasseur, 2000, **2**, 1319-1324.
22. M. Sathiya, G. Rousse, K. Ramesha, C. Laisa, H. Vezin, M. T. Sougrati, M.-L. Doublet, D. Foix, D. Gonbeau and W. J. N. m. Walker, 2013, **12**, 827.
23. R. Dedryvere, D. Foix, S. Franger, S. Patoux, L. Daniel and D. J. T. J. o. P. C. C. Gonbeau, 2010, **114**, 10999-11008.
24. A. Yamada, S.-C. Chung and K. Hinokuma, *Journal of the electrochemical society*, 2001, **148**, A224-A229.
25. T. Ohzuku, A. Ueda, M. Nagayama, Y. Iwakoshi and H. Komori, *Electrochimica Acta*, 1993, **38**, 1159-1167.
26. N. Yabuuchi and T. Ohzuku, *Journal of Power Sources*, 2003, **119**, 171-174.
27. L. Li, Y. Xu, X. Sun, R. Chang, Y. Zhang, X. Zhang and J. Li, *Advanced Energy Materials*, 2018, **8**, 1801064.
28. R. D. Shannon, *Acta crystallographica section A: crystal physics, diffraction, theoretical and general crystallography*, 1976, **32**, 751-767.
29. J. Niu, A. Kushima, X. Qian, L. Qi, K. Xiang, Y.-M. Chiang and J. Li, *Nano letters*, 2014, **14**, 4005-4010.
30. H. Liu, F. C. Strobridge, O. J. Borkiewicz, K. M. Wiaderek, K. W. Chapman, P. J. Chupas and C. P. Grey, *Science*, 2014, **344**, 1252817.
31. M. Z. Bazant, *Accounts of chemical research*, 2013, **46**, 1144-1160.
32. J. Lee, A. Urban, X. Li, D. Su, G. Hautier and G. Ceder, *Science*, 2014, **343**, 519-522.
33. A. Urban, I. Matts, A. Abdellahi and G. Ceder, *Advanced Energy Materials*, 2016, **6**, 1600488.
34. T. Ohzuku and A. Ueda, *Journal of The Electrochemical Society*, 1994, **141**, 2972-2977.
35. T. Ohzuku and Y. Makimura, *Chemistry letters*, 2001, **30**, 744-745.
36. J. L. Shi, D. D. Xiao, M. Ge, X. Yu, Y. Chu, X. Huang, X. D. Zhang, Y. X. Yin, X. Q. Yang and Y. G. Guo, *Advanced Materials*, 2018, **30**, 1705575.
37. H. Xu, S. Li,C. Zhang, X.L. Chen, W.J. Liu, Y.H. Zheng, Y. Xie, Y.H. Huang, J. Li, *Unpublished results.*